# Dalton Transactions

Accepted Manuscript






ROYAL SOCIETY OF CHEMISTRY

www.rsc.org/dalton

Journal Name

ARTICLE

# Preparation of α1- and α2-isomers of Mono-Ru-substituted Dawson-type Phosphotungstates with an Aqua Ligand and comparison of their Redox Potentials, Catalytic Activities, and Thermal stabilities with Keggin-type derivatives

Received 00th January 20xx,
Accepted 00th January 20xx

DOI: 10.1039/x0xx00000x

www.rsc.org/

Kensuke Nishiki,[a] Naoya Umehara,[a] Yusuke Kadota,[a] Xavier López,[b] Josep M. Poblet,[b] Charyle Ayingone Mezui,[c] Anne-Lucie Teillout,[c] Israël M. Mbomekalle,[c] Pedro de Oliveira,[c] Mayumi Miyamoto,[a] Tsuneji Sano,[a] and Masahiro Sadakane[a,d]*

Both the $\alpha_1$- and the $\alpha_2$-isomers of mono-ruthenium (Ru)-substituted Dawson-type phosphotungstates with a terminal aqua ligand, $[\alpha_1\text{-}P_2W_{17}O_{61}Ru^{III}(H_2O)]^{7-}$ (**$\alpha_1$-RuH$_2$O**) and $[\alpha_2\text{-}P_2W_{17}O_{61}Ru^{III}(H_2O)]^{7-}$ (**$\alpha_2$-RuH$_2$O**), were prepared in pure form by cleavage of the Ru-S bond of the corresponding DMSO derivatives, $[\alpha_1\text{-}P_2W_{17}O_{61}Ru(DMSO)]^{8-}$ (**$\alpha_1$-RuDMSO**) and $[\alpha_2\text{-}P_2W_{17}O_{61}Ru(DMSO)]^{8-}$ (**$\alpha_2$-RuDMSO**), respectively. Redox studies indicated that **$\alpha_1$-RuH$_2$O** and **$\alpha_2$-RuH$_2$O** show proton-coupled electron transfer (PCET), and the $Ru^{III}(H_2O)$ species was reversibly reduced to $Ru^{II}(H_2O)$ species and oxidized to the $Ru^{IV}(=O)$ species and further to the $Ru^{V}(=O)$ species in aqueous solution depending on the pH. Their redox potentials and thermal stabilities were compared with those of the corresponding α-Keggin-type derivatives ($[\alpha\text{-}XW_{11}O_{39}Ru(H_2O)]^{n-}$; X = $Si^{4+}$ ($n$ = 5), $Ge^{4+}$ ($n$ = 5), or $P^{5+}$ ($n$ = 4)). The basic electronic and redox features of Ru(L)-substituted Keggin- and Dawson-type heteropolytungstates (with L = $H_2O$ or $O^{2-}$) were analyzed by means of density functional calculations. Similar to the corresponding α-Keggin-type derivatives, both **$\alpha_1$-RuH$_2$O** and **$\alpha_2$-RuH$_2$O** show catalytic activity for water oxidation.

## Introduction

Heteropolytungstates are anionic mixed metal-oxide clusters with tungsten as the main metal, and they have attracted increasing interest because of their multi-electronic redox activities, photochemical properties, and acidic properties and are utilized as catalysts and functional materials.[1, 2] Recently, considerable attention has been directed towards mono-ruthenium(Ru)-substituted Keggin-type heteropolytungstates, where one $[W=O]^{4+}$ moiety in Keggin-type heteropolytungstate, $[XW_{12}O_{40}]^{n-}$ (X = P ($n$ = 3), Si and Ge ($n$ = 4)), is substituted by Ru (Figure 1a), because the Ru atom has unique redox properties, catalytic properties, and reactivities with organic inorganic compounds.[3, 4] Catalytic activities of mono-Ru-substituted Keggin-type heteropolytungstates, $[PW_{11}O_{39}Ru^{III}(H_2O)]^{4-}$, $[PW_{11}O_{39}Ru^{II}(DMSO)]^{5-}$ (DMSO: dimethyl sulfoxide), $[SiW_{11}O_{39}Ru^{III}(H_2O)]^{5-}$, $[SiW_{11}O_{39}Ru^{III}(DMSO)]^{5-}$ and $[GeW_{11}O_{39}Ru^{III}(H_2O)]^{5-}$, for oxidation of olefins,[5-7] water,[8-10] DMSO,[11, 12] and alcohols,[13, 14] reduction of DMSO[12] and carbon dioxide,[15] and oxidative C-C bond formation[16] have been reported. In these complexes, the Ru atom is coordinated by five oxygen atoms of the heteropolytungstate and one terminal ligand (Figure 1e). Mono-Ru-substituted heteropolytungstates with a terminal aqua ligand are important compounds because they produce $Ru^{V}$-oxo ($Ru^{V}(=O)$) species that are active in the oxidation of water,[8] alcohols,[14] and DMSO[11], and the labile water ligand is exchangeable with other organic and inorganic species to form Ru-pyridine,[12, 17, 18] Ru-pyrazine,[14] Ru-DMSO,[12, 19, 20] Ru-NO,[21] Ru-Cl,[22] Ru-CO,[23-25] Ru-olefine,[12] and Ru-μO derivatives.[26, 27] Similar to Keggin-type heteropolytungstates, the α-Dawson-type phosphotungstate, $[\alpha\text{-}P_2W_{18}O_{62}]^{6-}$, can incorporate transition metals. This compound is the second most common heteropolytungstate, containing two $PO_4$ tetrahedra formally surrounded by eighteen $WO_6$ octahedra (Figure 1b). This ellipsoidal structure presents two kinds of tungstens, so-called "cap" and "belt" tungstens, and substitution of the belt or cap

[a] Department of Applied Chemistry, Graduate School of Engineering, Hiroshima University, 1-4-1 Kagamiyama, Higashi-Hiroshima, 739-8527, Japan. Fax: +81 82 424 5494; Tel: +81 82 424 4456; E-mail: sadakane09@hiroshima-u.ac.jp
[b] Departament de Química Física i Inorgànica, Universitat Rovira i Virgili, Marcel·lí Domingo s/n, 43007 Tarragona, Spain.
[c] Laboratoire de Chimie-Physique, Université Paris-Sud, UMR 8000 CNRS, Orsay F-91405, France
[d] PRESTO, Japan Science and Technology Agency (JST), 4-1-8 Honcho, Kawaguchi, 332-0012, Japan.

Electronic Supplementary Information (ESI) available: [Fig. S1. ESI-MS spectra, Fig. S2. CVs of CVs of **$\alpha_1$-RuH$_2$O** and **$\alpha_2$-RuH$_2$O** in phosphate solution (pH 4.3), Fig. S3. IR of **$\alpha_1$-RuH$_2$O**, **$\alpha_2$-RuH$_2$O** , **$\alpha_1$-RuDMSO**, and **$\alpha_2$-RuDMSO**, Fig. S4. CVs of [$\alpha_1$- and $\alpha_2$-$P_2W_{17}O_{61}Ru(DMSO)$] produced by a reaction of **$\alpha_1$-RuH$_2$O** and **$\alpha_2$-RuH$_2$O** with DMSO, .Fig. S5. CVs of **$\alpha_1$-RuH$_2$O** with repeated scans, Fig. S6. Pourbaix diagram of **$\alpha_1$-RuH$_2$O**, **$\alpha_2$-RuH$_2$O**, $[SiW_{11}O_{39}Ru(H_2O)]^{n-}$, $[GeW_{11}O_{39}Ru(H_2O)]^{n-}$, and $[PW_{11}O_{39}Ru(H_2O)]^{n-}$, Fig. S7. HOMO of **$\alpha_1$-RuH$_2$O** and **$\alpha_2$-RuH$_2$O**, Fig. S8. TG-DTA of **$\alpha_1$-RuH$_2$O**, **$\alpha_2$-RuH$_2$O**, $[SiW_{11}O_{39}Ru(H_2O)]^{n-}$, $[GeW_{11}O_{39}Ru(H_2O)]^{n-}$, and $[PW_{11}O_{39}Ru(H_2O)]^{n-}$, Fig. S9. CVs of **$\alpha_1$-RuH$_2$O**, **$\alpha_2$-RuH$_2$O**, $[SiW_{11}O_{39}Ru(H_2O)]^{n-}$, $[GeW_{11}O_{39}Ru(H_2O)]^{n-}$, and $[PW_{11}O_{39}Ru(H_2O)]^{n-}$ heated at different temperatures.] See DOI: 10.1039/x0xx00000x

tungsten by Ru results in formation of the $\alpha_1$-isomer or the $\alpha_2$-isomer of mono-Ru-substituted Dawson-type phosphotungstates, $[P_2W_{17}O_{61}Ru(L)]^{(10-n)-}$ (L: ligand, *n* = valence of Ru), respectively (Figures 1c and 1d). Preparation of mono-Ru-substituted Dawson-type phosphotungstates with a terminal aqua ligand, $[P_2W_{17}O_{61}Ru^{III}(H_2O)]^{7-}$, is highly desired for the following reasons. (1) Redox potentials of $[P_2W_{17}O_{61}Ru^{V/IV}(=O)]^{7-/8-}$ are expected to be different from those of Keggin-type heteropolytungstates and different redox behaviours are expectable. (2) Different reactivity of the incorporated Ru to organic and inorganic compounds is expectable. (3) The $\alpha_1$-isomer is an enantiomer, though it exists as a racemic mixture, and reaction with chiral organic compounds produces diastereomers,[28, 29] and an enantiomerically pure one may act as a chiral catalyst.[30]

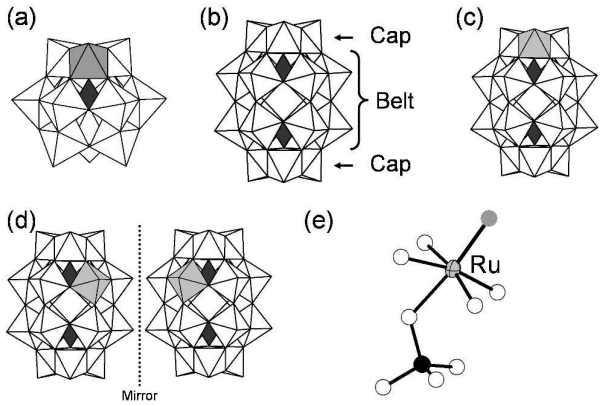


**Figure 1.** Polyhedral presentations of (a) a mono-Ru-substituted Keggin-type heteropolytungstate, (b) a Dawson-type phosphotungstate, $[\alpha\text{-}P_2W_{18}O_{62}]^{6-}$, (c) $\alpha_2$-isomer, and (d) $\alpha_1$-isomer of a mono-Ru-substituted Dawson-type phosphotungstate, $[P_2W_{17}O_{61}Ru]^{n-}$. White, black, and grey polyhedra represent $WO_6$ octahedron, $XO_4$ tetrahedron (X: P, Ge, or Si), and $RuO_5L$ (L: ligand) octahedron, respectively. (e) Ball-and-stick presentation of coordination environment of Ru. Oxygens, Ru, ligand, and heteroatom (X) are presented as white balls, crossed grey ball, grey ball, and black ball, respectively.

However, preparation of mono-Ru-substituted Dawson-type phosphotungstates with a terminal aqua ligand, $[P_2W_{17}O_{61}Ru^{III}(H_2O)]^{7-}$, in pure form has not yet been achieved. Pope's group[12] and Nomiya's group[31] reported preparation of the $\alpha_2$-isomer of mono-Ru($H_2O$)-substituted Dawson-type phosphotungstate, $[\alpha_2\text{-}P_2W_{17}O_{61}Ru^{III}(H_2O)]^{7-}$, by reaction of the $\alpha_2$-isomer of a mono lacunary Dawson-type phosphotungstate, $[\alpha_2\text{-}P_2W_{17}O_{61}]^{10-}$, with ruthenium sources and subsequent oxidations. However, they also reported that the isolated compound contained $[P_2W_{18}O_{62}]^{6-}$ as an impurity. Furthermore, isolation of the isomerically pure $\alpha_1$-isomer of mono-Ru-substituted Dawson-type phosphotungstate with a terminal aqua ligand, $[\alpha_1\text{-}P_2W_{17}O_{61}Ru^{III}(H_2O)]^{7-}$, has not been achieved.

We have recently reported the preparation of both isomerically pure $\alpha_1$- and $\alpha_2$-isomers of mono-Ru-substituted Dawson-type phosphotungstates with a DMSO molecule coordinating to the incorporated Ru, $[\alpha_1\text{-}P_2W_{17}O_{61}Ru^{II}(DMSO)]^{8-}$ (**$\alpha_1$-RuDMSO**) and $[\alpha_2\text{-}P_2W_{17}O_{61}Ru^{II}(DMSO)]^{8-}$ (**$\alpha_2$-RuDMSO**).[32]

Here, we present (1) preparations and characterizations of potassium salts of both $\alpha_1$- and $\alpha_2$-isomers of mono-Ru-substituted Dawson-type phosphotungstates with a terminal aqua ligand, $[\alpha_1\text{-}P_2W_{17}O_{61}Ru^{III}(H_2O)]^{7-}$ (**$\alpha_1$-RuH$_2$O**) and $[\alpha_2\text{-}P_2W_{17}O_{61}Ru^{III}(H_2O)]^{7-}$ (**$\alpha_2$-RuH$_2$O**), in pure form from the corresponding DMSO-coordinating species, **$\alpha_1$-RuDMSO** and **$\alpha_2$-RuDMSO**, respectively, (eqs. 1 and 2 and Scheme 1) by cleavage of Ru-S bonds, (2) comparison of redox potentials of five mono-Ru($H_2O$)-substituted heteropolytungstates, **$\alpha_1$-RuH$_2$O**, **$\alpha_2$-RuH$_2$O**, and $[\alpha\text{-}XW_{11}O_{39}Ru^{III}(H_2O)]^{n-}$ (X = Si (*n* = 5), Ge (*n* = 5), and P (*n* = 4)), (3) comparison of their thermal stabilities, and (4) their catalytic activities for water oxidation.

$$[\alpha_1\text{- or } \alpha_2\text{-}P_2W_{17}O_{61}Ru^{II}(DMSO)]^{8-} + H_2O \rightarrow [\alpha_1\text{- or } \alpha_2\text{-}P_2W_{17}O_{61}Ru^{II}(H_2O)]^{8-} + DMSO \quad (1)$$

$$[\alpha_1\text{- or } \alpha_2\text{-}P_2W_{17}O_{61}Ru^{II}(H_2O)]^{8-} + \text{air oxidation} \rightarrow [\alpha_1\text{- or } \alpha_2\text{-}P_2W_{17}O_{61}Ru^{III}(H_2O)]^{7-} \quad (2)$$

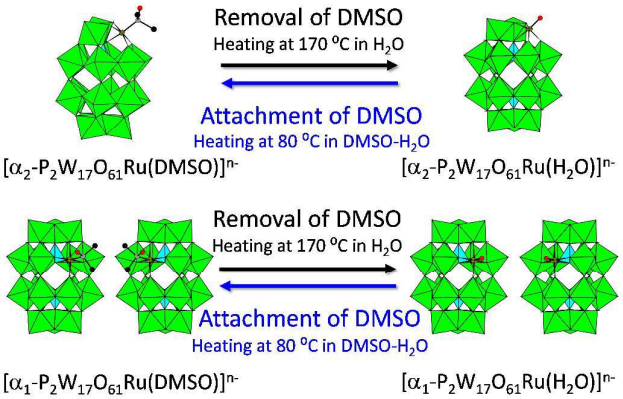


**Scheme 1.** Exchange between DMSO and $H_2O$ on Ru in mono-Ru-substituted Dawson-type phosphotungstates.

## Experimental

### Materials.

Homemade de-ionized water (Millipore, Elix) was used. The compounds $K_8[\alpha_1\text{-}P_2W_{17}O_{61}Ru(DMSO)]$ (**$\alpha_1$-RuDMSO**) and $K_8[\alpha_2\text{-}P_2W_{17}O_{61}Ru(DMSO)]$ (**$\alpha_2$-RuDMSO**) were prepared according to the published procedure and analyzed by cyclic voltammetry, $^1$H NMR, $^{31}$P NMR, and IR spectroscopy.[32] All other chemicals were reagent-grade and used as supplied.

### Synthetic procedures

**Preparation of $K_7[\alpha_1\text{-}P_2W_{17}O_{61}Ru^{III}(H_2O)]$.** $K_8[\alpha_1\text{-}P_2W_{17}O_{61}Ru(DMSO)]\cdot 22H_2O$ (0.158 g, 0.034 mmol) and water (5 mL) were poured into a 50 mL Teflon-lined autoclave. The autoclave was then placed in a conventional oven heated at 170 °C for 5 h. After the autoclave had been cooled to room temperature, the reaction mixture was filtrated. Subsequently,

20 mL of acetone was added to the filtrate and the solution was stirred at room temperature for 30 min. The produced dark-brown solid was filtered off, washed with 50 mL of acetone, and finally dried at 70 °C (0.110 g, 73% based on W).
IR (KBr): ν = 1090(m), 951 (s), 914 (s), 776 (m) $cm^{-1}$. Cyclic voltammogram (CV): $E_{1/2}$ ($Ru^{V/IV}$) = 855 mV, $E_{1/2}$ ($Ru^{IV/III}$) = 517 mV and $E_{1/2}$ ($Ru^{III/II}$) = –21 mV in 0.5 M $KH_2PO_4$ aqueous solution (pH 4.3). $^{31}P$ NMR ($D_2O$): (δ/ppm) −6.95. Elemental analysis: calculated for $K_7[P_2W_{17}O_{61}Ru(H_2O)]\cdot 0.4KCl\cdot 18H_2O$: H 0.90; P 1.26; W 63.65; Ru 2.06; K 5.89; Na 0; Cl 0.29%; found: H 0.72; P 1.24; W 63.4; Ru 2.13; K 6.23; Na 0.02; Cl 0.05%.
Negative ion MS ($CH_3CN$-$H_2O$): calculated for $[P_2W_{17}O_{61}RuOH_3]^{4-}$ m/z = 1070.9331, found m/z = 1070.9354 (Supporting Information, Figure S1(a) and (b))
**Preparation of $K_7[\alpha_2$-$P_2W_{17}O_{61}Ru^{III}(H_2O)]$.** $K_8[\alpha_2$-$P_2W_{17}O_{61}Ru(DMSO)]\cdot 16H_2O$ (0.158 g, 0.034 mmol) and water (10 mL) were poured into a 50 mL Teflon-lined autoclave. The autoclave was then placed in a conventional oven heated at 170 °C for 7.5 h. After the autoclave had been cooled to room temperature, 0.5 g of KCl was added to the filtrate and the solution was stirred at room temperature for 1 h. The solution was allowed to stand in a refrigerator overnight. The produced dark-brown solid was filtered off, washed with 50 mL of acetone, and finally dried at 70 °C (0.090 g, 57% based on W).
IR (KBr): ν = 1090 (m), 950 (s), 913 (s), 774 (m) $cm^{-1}$. CV: $E_{1/2}$ ($Ru^{IV/III}$) = 780 mV, $E_{1/2}$ ($Ru^{IV/III}$) = 457 mV and $E_{1/2}$ ($Ru^{III/II}$) = –95 mV in 0.5 M $KH_2PO_4$ aqueous solution (pH 4.3). $^{31}P$ NMR ($D_2O$): (δ/ppm) −15.23. Elemental analysis: calculated for $K_7[P_2W_{17}O_{61}Ru(H_2O)]$-0.1KCl-18$H_2O$: H 0.91; P 1.27; W 63.94; Ru 2.07; K 5.68; Na 0; Cl 0.07%; found: H 0.68; P 1.25; W 63.70; Ru 2.12; K 6.01; Na,0.02; Cl 0.06%.
Negative ion MS ($CH_3CN$-$H_2O$): calculated for $[P_2W_{17}O_{61}RuOH_3]^{4-}$ m/z = 1070.9331, found m/z = 1070.9357 (Supporting Information, Figures S1c and S1d).
**Water oxidation reaction.** A catalyst dissolved in 0.1 M $HNO_3$ solution was added to a 0.1 M $HNO_3$ solution containing cerium ammonium nitrate (CAN) (catalyst: 0.3 mM (6 μmol), CAN: 30 mM (600 μmol), total solution volume: 20 mL) at 20 ºC. The amount of generated oxygen was measured using a conventional gas burette. The amount of generated oxygen was also confirmed by using an $O_2$ sensor (HORIBA, OM-51) and GC-TCD (Shimadzu, GC8A) with a packed column (MS-5A, 2m, 3 mm i.d.).
**Other analytical techniques.** Infrared (IR) spectra were recorded on a NICOLET 6700 FT-IR spectrometer (Thermo Fisher Scientific) as KBr pellets. Cyclic voltammetry was performed on a CHI620D system (BAS Inc.) at ambient temperature. A glassy carbon working electrode (diameter, 3 mm), a platinum wire counter electrode, and an Ag/AgCl reference electrode (203 mV vs NHE at 25 °C) (3M NaCl, BAS Inc.) were used. Approximate formal potential values ($E_{1/2}$ values) were calculated from the CVs as the average of cathodic and anodic peak potentials for corresponding oxidation and reduction waves. UV-Vis spectra were recorded at ambient temperature using a 8453 UV-Vis spectrometer (Agilent) with a 1 cm quartz cell. UV-Vis measurements of electrochemically produced species were performed at ambient temperature using an 8453 UV-Vis spectrophotometer (Agilent) with a 0.5 mm electrochemical quartz cell (SEC-C, BAS Inc.). The working electrode was an Au-mesh electrode. A platinum wire counter electrode and Ag/AgCl reference electrode (203 mV vs NHE at 25 °C) (3M NaCl, BAS Inc.) were used. Potential was applied by means of an HAB-151 potentiostat (HOKUTO DENKO Ltd.). $^{31}P$ NMR spectra were recorded on a Varian system 500 (500 MHz) spectrometer (Agilent) (P resonance frequency: 202.333 MHz). The spectra were referenced to external 85% $H_3PO_4$ (0 ppm). Elemental analyses were carried out by Mikroanalytisches Labor Pascher (Remagen, Germany). High-resolution ESI-MS spectra were recorded on an LTQ Orbitrap XL (Thermo Fisher Scientific) with an accuracy of 3 ppm. Each sample (5 mg) was dissolved in 5 ml of $H_2O$, and the solutions were diluted by $CH_3CN$ (final concentration: ca. 10 μg/ml). TG-DTA measurements were performed with an SSC/5200 (Seiko Instruments) thermogravimetric analyzer. The sample (ca. 20 mg) was heated in a flow of air (50 ml/min) at 10 K/min from room temperature.
**Electronic structure calculations.** Density functional theory (DFT) calculations were performed with the ADF 2013[33-35] program applying either the restricted or unrestricted formalisms for closed- ($Ru^{II}$) or open-shell ($Ru^{III-V}$) electronic configurations, respectively. Total molecular energies were obtained on the geometries optimized with the BP86 functional[36-38] and triple-ζ + double polarization (TZ2P) Slater-type atomic basis sets for all atoms. Internal electrons were described by a frozen single Slater function (frozen core approximation) with relativistic effects included with the DIRAC module.[33] We accounted for the solvent effects of water with the *conductor-like screening model* (COSMO) in all calculations.[39-42] Including the solvent effects in the present calculations was crucial[43] as the gas phase approximation (isolated molecules without any stabilizing external agent) does not correctly reproduce the relative energies of a redox pair in solution. The final energies were obtained either from the above calculations (BP86 results) or by carrying out single point calculations with the hybrid B3LYP[44, 45] functional on the BP86-optimized geometries.
During geometry optimizations, the $H_2O$ and DMSO ligands can easily rotate over the Ru-L bond, the potential energy surface related to this geometric degree of freedom being quite flat. Thus, the optimization procedure might be tedious and lead to different local minima separated by small energies (< 1 kcal $mol^{-1}$). We therefore consider any of the structures found within this broad low-energy regions totally valid as equilibrium ones for the purpose of the present work.

## Results and discussion

**Preparation and structural characterization of $[\alpha_1$-$P_2W_{17}O_{61}Ru^{III}(H_2O)]^{7-}$ and $[\alpha_2$-$P_2W_{17}O_{61}Ru^{III}(H_2O)]^{7-}$.**
The isomerically pure $\alpha_1$- and $\alpha_2$-isomer of mono-Ru-substituted Dawson-type phosphotungstates with a DMSO ligand, $[\alpha_1$-$P_2W_{17}O_{61}Ru^{II}(DMSO)]^{8-}$ and $[\alpha_2$-$P_2W_{17}O_{61}Ru^{II}(DMSO)]^{8-}$, (denoted as **$\alpha_1$-RuDMSO** and **$\alpha_2$-**

**RuDMSO**, respectively), were heated at 170 °C in water. Figure 2 shows the CV of the reaction mixture of **$\alpha_1$-RuDMSO** after heating for 5 hours. Redox couples corresponding to **$\alpha_1$-RuDMSO** disappeared, being replaced by three new well-defined redox couples between 1000 mV and –200 mV. Similar changes were observed in the case of reaction with **$\alpha_2$-RuDMSO**. Addition of acetone or potassium chloride to the reaction solutions resulted in the production of dark-brown solids. CVs of both isolated solids show three well-defined redox couples between 1000 mV and –200 mV (Supporting Information, Figure S2), typical of mono-Ru-substituted heteropolytungstates with a terminal aqua ligand.[9]

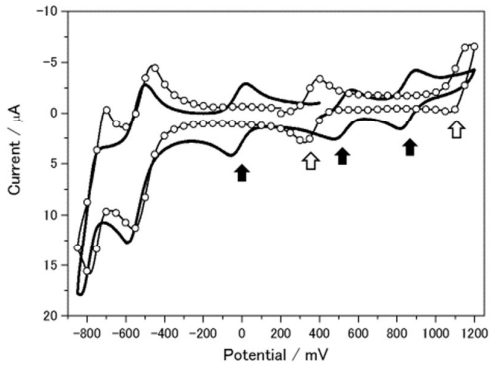


**Figure 2.** (black line) Cyclic voltammogram of the reaction mixture obtained after reaction of $[\alpha_1\text{-}P_2W_{17}O_{61}Ru^{II}(DMSO)]^{8-}$ in water at 170 °C for 5 hours. The reaction mixture (0.2 mL) was diluted with 0.54 M $KH_2PO_4$ (2.8 mL) to obtain a solution containing ca. 1.0 mM of Ru and 0.5 M $KH_2PO_4$ (pH 4.3). (black line with white balls) Cyclic voltammogram of isolate $K_8[\alpha_1\text{-}P_2W_{17}O_{61}Ru^{II}(DMSO)]$ (ca. 1.0 mM in 0.5 M $KH_2PO_4$ (pH 4.3)). The white and black arrows indicate redox pairs of $[\alpha_1\text{-}P_2W_{17}O_{61}Ru^{II}(DMSO)]^{8-}$ and new redox pairs generated after the reaction, respectively. Scan rate: 25 mV·s$^{-1}$.

IR spectra of both dark-brown solids are similar to those of **$\alpha_1$-RuDMSO** and **$\alpha_2$-RuDMSO**, indicating that both dark-brown solids have a Dawson-type phosphotungstate structure (Supporting Information, Figure S3). $^{31}$P NMR spectra of both dark-brown solids show only one signal (Figures 5b and 5e), indicating that the valence of Ru is 3+ and that one $^{31}$P NMR signal of phosphorus close to $Ru^{III}$ disappears due to a strong paramagnetic effect. Elemental analyses of both dark-brown solids reveal that the elemental ratios of P:W:Ru:K are 2:17:1:7, and the high resolution electro-spray ionization mass spectrum (HR-ESI-MS) of both compounds showed signals with the isotropic distribution which agrees with the pattern calculated for $[P_2W_{17}O_{61}RuOH_3]^{4-}$ within experimental accuracy (Supporting Information, Figure S1). These results indicate that the isolated dark-brown solids are the potassium salts of mono-$Ru^{III}$-substituted Dawson-type phosphotungstates with a terminal aqua ligand, $K_7[P_2W_{17}O_{61}Ru^{III}(H_2O)]$ (eqs. 1 and 2).

In order to confirm the isomeric structures of both dark-brown solids, we re-transferred the isolated $[P_2W_{17}O_{61}Ru^{III}(H_2O)]^{7-}$ to the corresponding DMSO compounds (eq. 3 and Scheme 1) and analysed them using $^{31}$P NMR. In the case of $[P_2W_{17}O_{61}Ru^{III}(H_2O)]^{7-}$ produced from **$\alpha_1$-RuDMSO**, the re-produced DMSO compound showed only two $^{31}$P NMR peaks (Figure 3c), which are the same as $^{31}$P NMR spectrum of **$\alpha_1$-RuDMSO** (Figure 3a). On the other hand, reaction of DMSO with $[P_2W_{17}O_{61}Ru^{III}(H_2O)]^{7-}$ prepared from **$\alpha_2$-RuDMSO** yield **$\alpha_2$-RuDMSO** (Figure 3f). The CV of a reaction mixture of DMSO and $[P_2W_{17}O_{61}Ru^{III}(H_2O)]^{7-}$ produced from **$\alpha_1$-RuDMSO** showed a single reversible redox couple typical of **$\alpha_1$-RuDMSO**, whereas a reaction mixture of DMSO and $[P_2W_{17}O_{61}Ru^{III}(H_2O)]^{7-}$ prepared from **$\alpha_2$-RuDMSO** showed a single reversible redox couple typical of **$\alpha_2$-RuDMSO** (Supporting Information Figure S4). These results confirm that isomerization does not occur during DMSO cleavage and re-production of Ru-DMSO species, and both $[\alpha_1\text{-}P_2W_{17}O_{61}Ru^{III}(H_2O)]^{7-}$ and $[\alpha_2\text{-}P_2W_{17}O_{61}Ru^{III}(H_2O)]^{7-}$ (denoted as **$\alpha_1$-RuH$_2$O** and **$\alpha_2$-RuH$_2$O**, respectively) are obtained in pure form.

$$[\alpha_1\text{- or } \alpha_2\text{-}P_2W_{17}O_{61}Ru^{III}(H_2O)]^{7-} + DMSO \rightarrow [\alpha_1\text{- or } \alpha_2\text{-}P_2W_{17}O_{61}Ru^{III}(DMSO)]^{7-} + H_2O \quad (3)$$

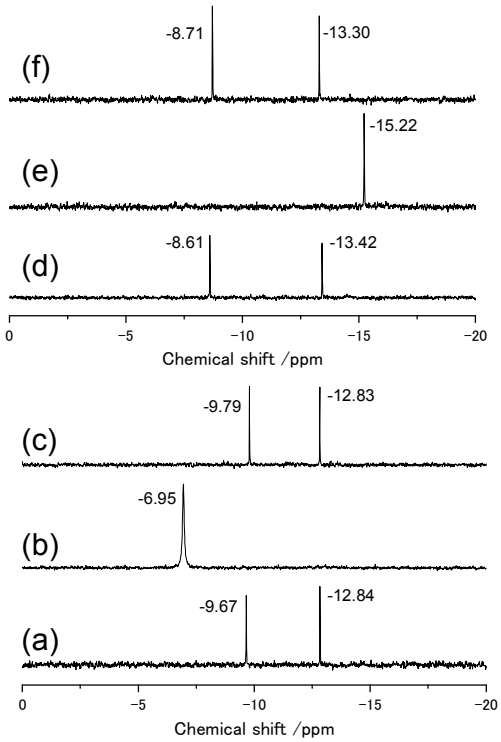


**Figure 3.** $^{31}$P NMR of (a) $K_8[\alpha_1\text{-}P_2W_{17}O_{61}Ru^{II}(DMSO)]$ (**$\alpha_1$-RuDMSO**), (b) the brown solid, $K_7[\alpha_1\text{-}P_2W_{17}O_{61}Ru^{III}(H_2O)]$ (**$\alpha_1$-RuH$_2$O**), obtained after reaction of $K_8[\alpha_1\text{-}P_2W_{17}O_{61}Ru^{II}(DMSO)]$ (**$\alpha_1$-RuDMSO**) in $H_2O$, (c) compound prepared by reaction of **$\alpha_1$-RuH$_2$O** with DMSO in $H_2O$, (d) $K_8[\alpha_2\text{-}P_2W_{17}O_{61}Ru(DMSO)]$ (**$\alpha_2$-RuDMSO**), (e) the brown solid $K_7[\alpha_2\text{-}P_2W_{17}O_{61}Ru^{III}(H_2O)]$ (**$\alpha_2$-RuH$_2$O**), obtained after reaction of $K_8[\alpha_2\text{-}P_2W_{17}O_{61}Ru^{II}(DMSO)]$ (**$\alpha_2$-RuDMSO**) in $H_2O$, and (f) compound prepared by reaction of **$\alpha_2$-RuH$_2$O** with DMSO in $H_2O$. Samples (ca. 4.6 mg) were dissolved in $D_2O$ (1 mL). In the case of (a), (c), (d), and (f), ascorbic acid (ca. 2 mg) was added to produce $Ru^{II}$DMSO species.

The broader $^{31}$P NMR signal of **$\alpha_1$-RuH$_2$O** compared to that of **$\alpha_2$-RuH$_2$O** (half-peak widths of 18.2 and 4.5 Hz, respectively) is explained by a stronger paramagnetic effect of $Ru^{III}$ in **$\alpha_1$-RuH$_2$O**. The distance between paramagnetic $Ru^{III}$ and the

observed phosphorous in **$\alpha_1$-RuH$_2$O** is shorter than that in **$\alpha_2$-RuH$_2$O**. Distances between the Ru atom and the most distant P estimated using single crystal structure data of **$\alpha_1$-RuDMSO** and **$\alpha_2$-RuDMSO** are ca. 5.2 Å and ca. 7.1 Å, respectively.[32]

Cyclic voltammograms of both **$\alpha_1$-RuH$_2$O** and **$\alpha_2$-RuH$_2$O** show three well-defined redox couples between 1000 mV and –200 mV (Supporting Information, Figure S2) typical of mono-Ru(H$_2$O)-substituted heteropolytungstates.[9, 27] UV-Vis spectra of electrochemically generated Ru$^{II}$, Ru$^{III}$, Ru$^{IV}$, and Ru$^{V}$ species of both $\alpha_1$-RuH$_2$O and $\alpha_2$-RuH$_2$O are presented in Figure 4. UV-Vis spectra of solutions electrolyzed at –190 mV and –290 mV for **$\alpha_1$-RuH$_2$O** and **$\alpha_2$-RuH$_2$O**, respectively, are similar to those of mono-Ru(H$_2$O)-substituted heteropolytungstates with Ru$^{II}$ (Figure 4).[12, 27] These results confirm that the three electron-transfer processes between 1000 mV and –200 mV correspond to one-electron transfer of Ru$^{III/II}$, Ru$^{IV/III}$, and Ru$^{V/IV}$, and re-confirm that the valence of the Ru atom in the isolated solid is 3+. The redox potentials of Ru$^{III/II}$ of **$\alpha_1$-RuDMSO** and **$\alpha_2$-RuDMSO** undergo a negative shift by converting to **$\alpha_1$-RuH$_2$O** and **$\alpha_2$-RuH$_2$O** (Figure 2 and Table 1), and the Ru$^{II}$(H$_2$O) species produced after cleavage of the Ru-DMSO bond is oxidized to Ru$^{III}$(H$_2$O) species by air in the autoclave and during the workup procedure (eq. 2).

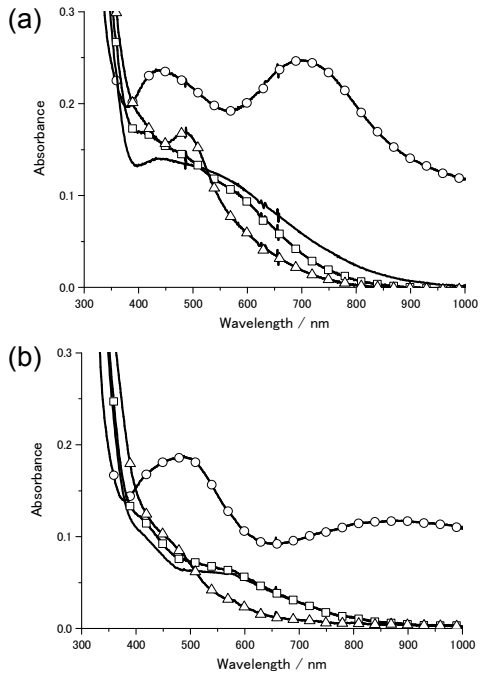


**Figure 4.** UV-Vis spectra of (a) **$\alpha_1$-RuH$_2$O** and (b) **$\alpha_2$-RuH$_2$O**. (black solid) isolated complex (Ru$^{III}$(H$_2$O) species), (black solid with open circles) electrochemically generated Ru$^{II}$(H$_2$O) species, (black solid with open squares) Ru$^{IV}$(=O) species, and (black solid with open triangles) Ru$^{V}$(=O) species. Concentration of the complex is ca. 1 mM and solvent is 0.5 M KH$_2$PO$_4$ (pH 4.3).

**Electrochemical study of [$\alpha_1$-P$_2$W$_{17}$O$_{61}$Ru$^{III}$(H$_2$O)]$^{7-}$ and [$\alpha_2$-P$_2$W$_{17}$O$_{61}$Ru$^{III}$(H$_2$O)]$^{7-}$ ($\alpha_1$-RuH$_2$O and $\alpha_2$-RuH$_2$O) in aqueous solution.** A first characterisation of the two isomers was carried out in 0.2M Na$_2$SO$_4$ + H$_2$SO$_4$ (pH 3.0) for which the redox behaviour of the respective parent compounds $\alpha_1$-[P$_2$W$_{17}$O$_{61}$]$^{10-}$ and $\alpha_2$-[P$_2$W$_{17}$O$_{61}$]$^{10-}$ is well known.[46]

The present study reveals that the Ru$^{III}$ centre in the $\alpha_1$ position is easier to reduce than the Ru$^{III}$ centre in the $\alpha_2$ position. However, as far as the first reduction wave corresponding to two two-electron transfers to W by comparison of redox currents.[47] of the W$^{VI}$ centres of the tungstic scaffold of the P$_2$W$_{17}$O$_{61}$ Dawson fragment is concerned, it turns out that the $\alpha_2$-isomer is easier to reduce than the $\alpha_1$-isomer (Figure 5a).

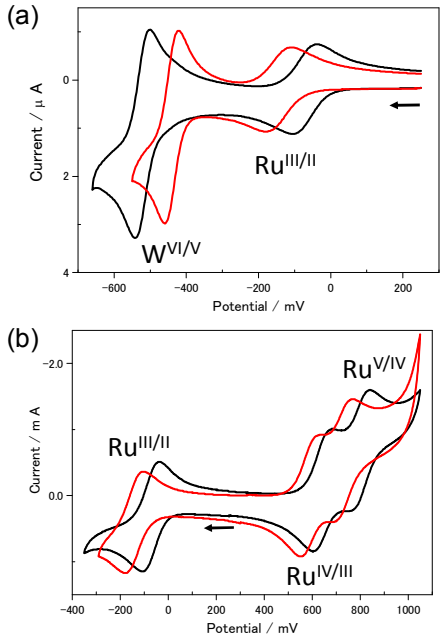


**Figure 5.** Cyclic voltammograms of (black) **$\alpha_1$-RuH$_2$O** and (red) **$\alpha_2$-RuH$_2$O** in 0.2M Na$_2$SO$_4$ + H$_2$SO$_4$ (pH 3.0). POM concentration: 2.5×10$^{-4}$ M. Scan rate: 10 mV·s$^{-1}$. Working electrode: EPG; counter electrode: Pt; reference electrode: SCE. (a) The potential was scanned in the negative direction and restricted to the reduction wave of Ru$^{III}$ and to the 1$^{st}$ reduction wave of the W centres. (b) The potentials was scanned in the negative direction and restricted to the reduction wave of Ru$^{III}$, and then scanned in the positive direction beyond the wave assigned to the formation of Ru$^{V}$.

The redox behaviour of the **$\alpha_1$-RuH$_2$O** and the **$\alpha_2$-RuH$_2$O** is closer to that of V$^{IV}$, V$^{V}$, Mo$^{VI}$ and Re$^{V}$-substituted compounds,[48-52] in which the M-substituted cation is surrounded by 6 oxygen atoms, 5 of which belong to the Dawson tungstic scaffold and the 6$^{th}$ is a terminal oxo group, i.e. having a double bond with M. These compounds have the general formula [P$_2$W$_{17}$O$_{61}$M=O], with M = V$^{IV}$, V$^{V}$, Mo$^{VI}$, or Re$^{V}$, the M-substituted cation in the $\alpha_1$ position being always easier to reduce than the one in the $\alpha_2$ position, irrespective of the pH of the medium.[53]

Another observation that deserves to be reported is that in 0.2M Na$_2$SO$_4$ + H$_2$SO$_4$ (pH 3.0) the Ru$^{III}$ and Ru$^{IV}$ centers in the $\alpha_2$ position, **$\alpha_2$-RuH$_2$O**, are always easier to oxidise than in the $\alpha_1$ position, **$\alpha_1$-RuH$_2$O** (Figure 5b).

Cyclic voltammograms of **$\alpha_1$-RuH$_2$O** and **$\alpha_2$-RuH$_2$O** in solutions with different pH values are presented in Figure 6. All redox couples of Ru and W depend on the pH values of the solutions.

It should be noted that the redox waves of $Ru^{IV/III}$ become less reversible when pH is 6.0 (Figures 6 (a) and (b) blue). These redox couples becomes more reversible when the cyclic voltammetry scans are repeated (Supporting Information, Figure S5). This kind of CV shape change with repeated scanning has been reported in cyclic voltammograms of $[SiW_{11}O_{39}Mn(H_2O)]^{n-}$ in phosphate buffer where exchange of $H_2O$ and phosphate (eq. 4) might be a reason of the shape change.[54] It is also known that many organic compounds and $Cl^-$ can replace $H_2O$ coordinated to Ru in $[XW_{11}O_{39}Ru]$.[12, 17, 19-24] Further investigations to understand this phenomenon is now undergoing in our group.

$$[P_2W_{17}O_{61}Ru^{III}(H_2O)]^{7-} + \text{phosphate}^{n-} \rightleftarrows [P_2W_{17}O_{61}Ru^{III}(\text{phosphate})]^{(7+n)-} + H_2O \quad (4)$$

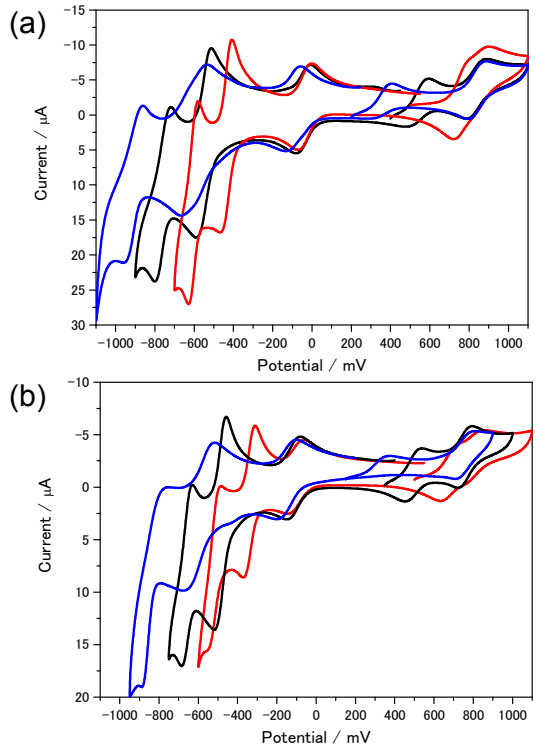


**Figure 6.** Cyclic voltammograms of (a) **$\alpha_1$-$RuH_2O$** and (b) **$\alpha_2$-$RuH_2O$** in solution of pH values of (red) 2, (black) 4, and (blue) 6. pH values are adjusted using Britton-Robinson buffer (0.2 M NaOH was added to a solution containing $CH_3CO_2H$ (0.04 M), $H_3PO_4$ (0.04 M), and $B(OH)_3$ (0.04 M)) with 0.5 M $NaNO_3$. POM concentration: $1.0\times10^{-3}$ M for **$\alpha_1$-$RuH_2O$** and $7.5\times10^{-4}$ M for **$\alpha_2$-$RuH_2O$**. Scan rate: 25 mV·$s^{-1}$.

Apparent redox potentials of each redox couple are plotted vs. pH of the solution in Figure 7. The pH dependence of each redox potential is similar to that of other mono-Ru-substituted heteropolytungstates with a terminal aqua ligand.[9, 27] When a redox potential is independent of the pH, the redox couple is not accompanied by deprotonation/protonation. On the other hand, when a redox potential depends on the pH with slopes of ca. –59 mV/pH and –118 mV/pH, the corresponding oxidation/reduction is accompanied by one- and two-proton deprotonation/protonation, respectively.[47, 55]

The apparent redox potential of $Ru^{III/II}$ is pH-independent between pH ca. 1.7 and ca. 5.2 for **$\alpha_1$-$RuH_2O$** and between pH ca. 2.1 and 5.3 for **$\alpha_2$-$RuH_2O$**, indicating that neither of the $Ru^{III/II}$ redox couples includes protonation and deprotonation (eq. 5). When the pHs of the solutions are lower than these ranges, the apparent redox potentials shift to more positive potentials with slopes of ca. –36 mV/pH for **$\alpha_1$-$RuH_2O$** and –46 mV/pH for **$\alpha_2$-$RuH_2O$**, indicating that the $\alpha_1$-isomer and $\alpha_2$-isomer of $[P_2W_{17}O_{61}Ru^{II}(H_2O)]^{8-}$ are one-proton protonated (eq. 6). When the pH of the solution is higher than this range, the apparent redox potentials are negatively shifted with slopes of ca. –53 mV/pH for **$\alpha_1$-$RuH_2O$** and –46 mV/pH for **$\alpha_2$-$RuH_2O$**. This phenomena might be explained by the fact that the $\alpha_1$-isomer and $\alpha_2$-isomer of $[P_2W_{17}O_{61}Ru^{III}(H_2O)]^{8-}$ is one-proton de-protonated with pKa values of ca. 5.2 and 5.3, respectively (eqs. 7 and 8). However, we should also consider a possible phosphate coordination mentioned above, and further investigation is needed to confirm the pKa values.

$$[P_2W_{17}O_{61}Ru^{III}(H_2O)]^{7-} + e^- \rightleftarrows [P_2W_{17}O_{61}Ru^{II}(H_2O)]^{8-} \quad (5)$$
(pH: ca. 1.7 ~ ca. 5.2 for the $\alpha_1$-isomer and ca. 2.1 ~ ca. 5.3 for the $\alpha_2$-isomer)

$$[P_2W_{17}O_{61}Ru^{III}(H_2O)]^{7-} + e^- + H^+ \rightleftarrows H[P_2W_{17}O_{61}Ru^{II}(H_2O)]^{7-} \quad (6)$$
(pH: ~ca. 1.7 for the $\alpha_1$-isomer and ~ca. 2.1 for the $\alpha_2$-isomer)

$$[P_2W_{17}O_{61}Ru^{III}(OH)]^{7-} + e^- + H^+ \rightleftarrows [P_2W_{17}O_{61}Ru^{II}(H_2O)]^{7-} \quad (7)$$
(pH: ca. 5.2 ~ for the $\alpha_1$-isomer and ca. 5.3 ~ for the $\alpha_2$-isomer)

$$[P_2W_{17}O_{61}Ru^{III}(H_2O)]^{7-} \rightleftarrows [P_2W_{17}O_{61}Ru^{III}(OH)]^{8-} + H^+ \quad (8)$$
(pKa: ca. 5.2 for the $\alpha_1$-isomer and ca. 5.3 for the $\alpha_2$-isomer)

The apparent redox potential of $Ru^{IV/III}$ is pH-dependent with a slope of ca. –69 mV/pH and -64 mV/pH when the solution pH is higher than ca. 5.2 for the $\alpha_1$-isomer and ca. 5.3 for the $\alpha_1$-isomer, respectively, indicating that $[P_2W_{17}O_{61}Ru^{III}(OH)]^{8-}$ is oxidized to $[P_2W_{17}O_{61}Ru^{IV}(=O)]^{8-}$ (eq. 9). When the solution pH is in the ranges of ca. 2.5 - 5.2 and ca. 2.7 - 5.3 for the $\alpha_1$-isomer and $\alpha_2$-isomer, respectively, the apparent redox potentials of $Ru^{IV/III}$ are shifted with slopes of ca. –112 mV/pH for **$\alpha_1$-$RuH_2O$** and –108 mV/pH for **$\alpha_2$-$RuH_2O$**, indicating that oxidation of $Ru^{III}(H_2O)$ is accompanied by two-proton deprotonation to form $Ru^{IV}(=O)$ species in these pH ranges (eq. 10). When the solution pH is between ca. 1.5 and ca. 2.5 for the $\alpha_1$-isomer and between ca. 1.5 and ca. 2.7 for the $\alpha_2$-isomer, the slope changes to ca. –74 mV/pH, and therefore the $Ru^{IV/III}$ redox couples are accompanied by one-proton transfer (eq. 11). Furthermore, for solution with pH values lower than 1.5 for both isomers, the $Ru^{IV/III}$ apparent redox potentials are pH-independent, indicating that no proton transfer is involved in the redox couple (eq. 12). These results indicate that $[P_2W_{17}O_{61}Ru^{IV}(H_2O)]^{6-}$ loses one proton with pKa values of ca. 1.5 for both the $\alpha_1$-isomer and the $\alpha_2$-isomer (eq. 13) and $[P_2W_{17}O_{61}Ru^{IV}(OH)]^{7-}$ loses one proton with pKa values of ca. 2.5 for the $\alpha_1$-isomer and ca. 2.7 for the $\alpha_2$-isomer (eq. 14).

$$[P_2W_{17}O_{61}Ru^{IV}(=O)]^{8-} + e^- + H^+ \rightleftarrows [P_2W_{17}O_{61}Ru^{III}(OH)]^{8-} \quad (9)$$

(pH: ca. 5.2 ~ for the $\alpha_1$-isomer and ca. 5.3 ~ for the $\alpha_2$-isomer)

$[P_2W_{17}O_{61}Ru^{IV}(=O)]^{8-} + e^- + 2H^+ \rightleftarrows [P_2W_{17}O_{61}Ru^{III}(H_2O)]^{7-}$ (10)
(pH: ca. 2.5 ~ 5.2 for the $\alpha_1$-isomer and ca. 2.7 ~ 5.3 for the $\alpha_2$-isomer)

$[P_2W_{17}O_{61}Ru^{IV}(OH)]^{7-} + e^- + H^+ \rightleftarrows [P_2W_{17}O_{61}Ru^{III}(H_2O)]^{7-}$ (11)
(pH: ca. 1.5 ~ 2.5 for the $\alpha_1$-isomer and ca. 1.5 ~ 2.7 for the $\alpha_2$-isomer)

$[P_2W_{17}O_{61}Ru^{IV}(H_2O)]^{6-} + e^- \rightleftarrows [P_2W_{17}O_{61}Ru^{III}(H_2O)]^{7-}$ (12)
(pH: ca. ~ 1.5 for both the $\alpha_1$-isomer and $\alpha_2$-isomer)

$[P_2W_{17}O_{61}Ru^{IV}(H_2O)]^{6-} \rightleftarrows [P_2W_{17}O_{61}Ru^{IV}(OH)]^{7-} + H^+$ (13)
(pKa: ca. 1.5 for the both $\alpha_1$-isomer and $\alpha_2$-isomer)

$[P_2W_{17}O_{61}Ru^{IV}(OH)]^{7-} \rightleftarrows [P_2W_{17}O_{61}Ru^{IV}(=O)]^{8-} + H^+$ (14)
(pKa: ca. 2.5 for the $\alpha_1$-isomer and ca. 2.7 for the $\alpha_2$-isomer)

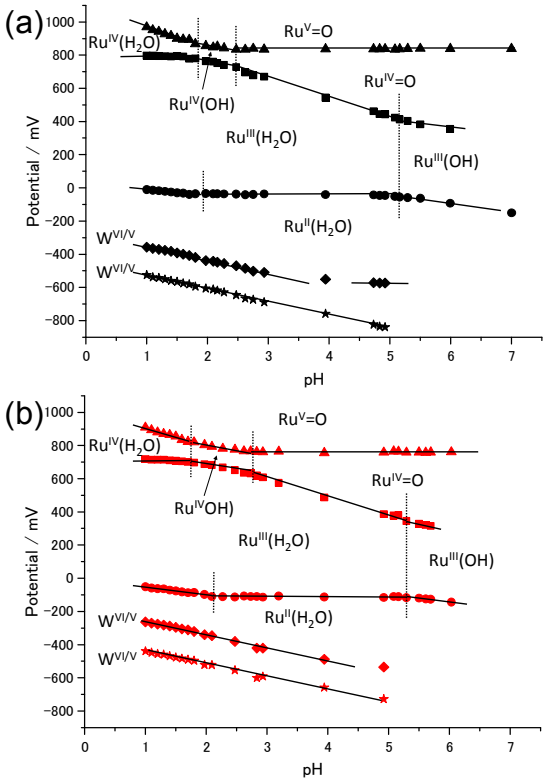


**Figure 7.** Pourbaix diagram (apparent redox potentials against pH of the solution) of (a) **$\alpha_1$-RuH$_2$O** and (b) **$\alpha_2$-RuH$_2$O**. Britton-Robinson buffer (0.2 M NaOH was added to a solution containing $CH_3CO_2H$ (0.04 M), $H_3PO_4$ (0.04 M), and $B(OH)_3$ (0.04 M)) with 0.5 M $NaNO_3$ for pH range of 1.8-7.0 and 0.5 M $NaHSO_4$ + 0.5 M $H_2SO_4$ for pH less than 1.8.

The apparent redox potential of $Ru^{V/IV}$ is pH-independent when the solution pH is higher than 2.5 for the $\alpha_1$-isomer and higher than 2.7 for the $\alpha_2$-isomer but shifts to more positive potentials with slopes of ca. –69 mV/pH for **$\alpha_1$-RuH$_2$O** and –65 mV/pH for **$\alpha_2$-RuH$_2$O** when pH of the solution is lower than these pH values. Furthermore, the apparent redox potentials of $Ru^{V/IV}$ are pH-dependent with slopes of ca. –125 mV/pH for **$\alpha_1$-RuH$_2$O** and ca. –104 mV/pH for **$\alpha_2$-RuH$_2$O** when the solution pH is lower than 1.5. These results indicate that $[P_2W_{17}O_{61}Ru^{V}(=O)]^{7-}$ is produced at all of the examined pH values (eqs. 15-17).

$[P_2W_{17}O_{61}Ru^{V}(=O)]^{7-} + e^- \rightleftarrows [P_2W_{17}O_{61}Ru^{IV}(=O)]^{8-}$ (15)
(pH: ca. 2.5 ~ for the $\alpha_1$-isomer and ca. 2.7 ~ for the $\alpha_2$-isomer)

$[P_2W_{17}O_{61}Ru^{V}(=O)]^{7-} + e^- + H^+ \rightleftarrows [P_2W_{17}O_{61}Ru^{IV}(OH)]^{7-}$ (16)
(pH: ca. 1.5 ~ 2.5 for the $\alpha_1$-isomer and ca. 1.5 ~ 2.7 for the $\alpha_2$-isomer)

$[P_2W_{17}O_{61}Ru^{V}(=O)]^{7-} + e^- + 2H^+ \rightleftarrows [P_2W_{17}O_{61}Ru^{IV}(H_2O)]^{6-}$ (17)
(pH: ca. ~ 1.5 for the both $\alpha_1$-isomer and $\alpha_2$-isomer)

Apparent redox potentials of 2-electron reduction of W of both **$\alpha_1$-RuH$_2$O** and **$\alpha_2$-RuH$_2$O** shift with slopes of ca. 60 mV/pH, indicating that 2-proton protonation occurs by reductions. The first reduction wave of the W of **$\alpha_1$-RuH$_2$O** splits and gives rise to two single-electron waves very close to each other when pH is higher than ca. 4.0 (Figure 6(a)), because the one-electron reduced species has pKa value of ca. 4.0.

The apparent redox potentials of Ru center are summarized in Table 1 together with those of mono-Ru-substituted α-Keggin-type heteropolytungstates with a terminal aqua ligand measured in the same media (Supporting Information, Figure S6) and mono-Ru-substituted heteropolytungstates with a DMSO ligand.[10, 19, 20, 32] The order of apparent redox potentials of $Ru^{III/II}(H_2O)$ species is $[\alpha\text{-}SiW_{11}O_{39}Ru^{III/II}(H_2O)]^{5/6-}$ < $[\alpha\text{-}GeW_{11}O_{39}Ru^{III/II}(H_2O)]^{5/6-}$ < $[\alpha_2\text{-}P_2W_{17}O_{61}Ru^{III/II}(H_2O)]^{7/8-}$ < $[\alpha_1\text{-}P_2W_{17}O_{61}Ru^{III/II}(H_2O)]^{7/8-}$ < $[\alpha\text{-}PW_{11}O_{39}Ru^{III/II}(H_2O)]^{4/5-}$, which coincides with the order of redox potentials of $Ru^{III/II}$(DMSO) species. The order of apparent redox potentials of $Ru^{V/IV}$(=O) species is $[\alpha\text{-}SiW_{11}O_{39}Ru^{V/IV}(=O)]^{5/6-}$ = $[\alpha_2\text{-}P_2W_{17}O_{61}Ru^{V/IV}(=O)]^{7/8-}$ < $[\alpha\text{-}GeW_{11}O_{39}Ru^{V/IV}(=O)]^{5/6-}$ < $[\alpha_1\text{-}P_2W_{17}O_{61}Ru^{V/IV}(=O)]^{7/8-}$ < $[\alpha\text{-}PW_{11}O_{39}Ru^{V/IV}(=O)]^{4/5-}$, and this order is slightly different from that of $Ru^{III/II}(H_2O)$ species.

**Table 1.** Summary of apparent redox potentials of mono-Ru-substituted heterpolytungstates.

| | $[XW_{11}O_{39}Ru(H_2O)]^{n-}$ | | | $[P_2W_{17}O_{61}Ru(H_2O)]^{n-}$ | |
|---|---|---|---|---|---|
| | $Si^{4+}$ | $Ge^{4+}$ | $P^{5+}$ | α1-iso. | α2-iso. |
| Redox potentials[a)] | | | | | |
| $Ru^{V/IV}(=O)$[b)] | 757 | 783 | 929 | 837 | 756 |
| $Ru^{IV/III}(H_2O)$[c)] | 714 | 793 | – | 796 | 719 |
| $Ru^{III/II}(H_2O)$[b)] | -215 | -163 | 13 | -41 | -113 |
| | $[XW_{11}O_{39}Ru(DMSO)]^{n-}$ | | | $[P_2W_{17}O_{61}Ru(DMSO)]^{n-}$ | |
| | $Si^{4+, d)}$ | $Ge^{4+, e)}$ | $P^{5+, f)}$ | α1-iso.[g)] | α2-iso.[g)] |
| Redox potentials | | | | | |
| $Ru^{IV/III}$(DMSO) | 1176 | 1218 | 1388 | 1138 | 1148 |
| $Ru^{III/II}$(DMSO) | 181 | 238 | 376 | 357 | 248 |

[a)] The redox potential was measured in Britton-Robinson buffer with 0.5 M NaNO3 for pH range of 1.8-7.0 and 0.5 M NaHSO4 + 0.5 M H2SO4 solution for pH less than 1.8, and values are against an Ag/AgCl (3M NaCl) reference electrode (ca. 202 mV vs. NHE). b) pH 3.9. c) pH 1.0. d) values in ref 18, e) values in ref 19, [f)] values in ref 8, and [g)] values in ref 32.

**DFT calculations.** This section supplements the electrochemical study with DFT calculations[45] for compounds containing L = aqua/oxo and DMSO to better understand the redox waves observed in cyclic voltammetry measurements. As shown in previous works,[53, 56] the computed electronic energy differences ($\Delta E$, eV units) can be semi-quantitatively linked to features and trends of measured redox potentials ($\Phi$, V units) through the Faraday constant owing to the equation $\Delta E \approx \Delta G = -nF\Phi$. Thermal corrections are not accounted for in the present work. Reduction and oxidation energies (RE or OE, respectively) can be computed through:

POMox + e $\rightarrow$ POMred RE = $E$(POMred) – $E$(POMox)

POMred $\rightarrow$ POMox + e OE = $E$(POMox) – $E$(POMred)

with the energy of the free electron equal to zero. If these two processes involve the same POMox and POMred species, they are of course related by RE = –OE. From this relation, if a reduction process entails a very negative (exothermic, favorable) RE, the opposite (oxidation) process will be characterized by a very positive (endothermic, unfavorable) OE. Thus, the most favored oxidation (reduction) processes feature the least (most) positive $\Phi$ values.

In the pseudo-octahedral field generated by the ligands surrounding the Ru centre in $Ru^{II}$-$Ru^{V}$ species, the calculations assume low spin Ru ions,[57] that is, partially filled $t_{2g}$-like orbitals and empty $e_g$-like orbitals (Figure 8).

Table 2 shows the computed OEs for the proton-decoupled $Ru^{V/IV}$(=O) and $Ru^{III/II}$($H_2O$) processes with two different functionals and for $Ru^{IV/III}$(DMSO) and $Ru^{III/II}$(DMSO) derivatives to highlight the ligand effect. On the other hand, the $Ru^{IV}/Ru^{III}$ process is highly pH-dependent as deduced from the Pourbaix diagrams shown in Figure 7. A thorough theoretical discussion on such an intricate process will be given in a forthcoming work. In Ru(DMSO) compounds, OEs are larger than Ru($H_2O$/=O) ones, and the greater tendency of Ru(DMSO) compounds to feature lower oxidation states than those of Ru($H_2O$) compounds is thus theoretically confirmed. An additional calculation for the $PW_{11}Ru^{IV}$(DMSO) $\rightarrow$ $PW_{11}Ru^{V}$(DMSO) + e oxidation process (not reported in Table 1) predicts that the associated OE reaches ~6.0 eV (that is, a potential of more than +1.5 V vs Ag/AgCl). This is in agreement with the lack of Ru/IV)/Ru(V) electrochemical wave for L = DMSO. In line with this, the computed orbital energies for $\alpha_1/\alpha_2$-$P_2W_{17}$Ru(IV) compounds with L = DMSO show that the HOMO orbitals lie at –5.5 eV whereas, for L = oxo, the HOMO energies are about –4.6 eV (BP86 functional).

Let us enumerate some theoretical facts for L = $H_2O$/oxo compounds to attest a correct understanding of the redox waves: (i) the order of precedence of redox processes (smaller to larger OE/potential), (ii) the separation between the $Ru^{V/IV}$(=O) and $Ru^{III/II}$($H_2O$) waves. Depending on the type of compound, the measured separations are found to be ~970-920 mV and ~880-870 mV for Keggin and Dawson compounds, respectively. The homologous computed energy separations are ca. 1000 meV and 900 meV, that is, for Dawson compounds they are 100 mV smaller. (iii) The $Ru^{V/IV}$ and $Ru^{III/II}$ waves in Dawson derivatives are mutually closer than those in Keggin anions. This trend is concomitant with the larger size of the Dawson compound, which undergoes a slightly smaller potential shift upon oxidation. (iv) Finally, looking at the range of values spanned by $Ru^{III/II}$ OEs as we move from $PW_{11}Ru$ to $SiW_{11}Ru$, 228 meV at the BP86 and 243 meV at the B3LYP levels, these reproduce the observed 228 mV very well. Such a value resembles, although not exactly reproduces, the slope of 180 mV/charge unit reported by Pope for $[X^{n+}W_{12}O_{40}]$ Keggin anions.[58] Within this family of compounds, and by virtue of their corresponding molecular charges, Keggin and $\alpha_1$-Dawson phosphates are the strongest oxidants irrespective of L, whereas silicate is the weakest oxidant. Summarizing, the DFT results reproduce the experimental findings, allowing us to clearly connect measured CV waves with computed redox energies.

**Table 2.** Computed BP86 and B3LYP oxidation energies[a] (OEs) for Ru compounds with terminal aqua/oxo[b] and DMSO[c] ligands.

| | $[XW_{11}O_{39}Ru(L)]^{n-}$ | | | $[P_2W_{17}O_{61}Ru(L)]^{n-}$ | |
|---|---|---|---|---|---|
| | $Si^{4+}$ | $Ge^{4+}$ | $P^{5+}$ | $\alpha_1$-iso. | $\alpha_2$-iso. |
| BP86 | | | | | |
| $Ru^{V/IV}$(=O) | 4.699 | 4.782 | 4.917 | 4.849 | 4.694 |
| $Ru^{III/II}$($H_2O$) | 4.045 | 4.130 | 4.273 | 4.235 | 4.131 |
| $Ru^{IV/III}$(DMSO) | 5.165 | 5.255 | 5.434 | 5.026 | 5.107 |
| $Ru^{III/II}$(DMSO) | 4.283 | 4.379 | 4.498 | 4.516 | 4.345 |
| B3LYP | | | | | |
| $Ru^{V/IV}$(=O) | 4.683 | 4.777 | 4.906 | 4.773 | 4.681 |
| $Ru^{III/II}$($H_2O$) | 3.654 | 3.749 | 3.897 | 3.942 | 3.709 |
| $Ru^{IV/III}$(DMSO) | 5.091 | 5.188 | 5.402 | 4.961 | 5.051 |
| $Ru^{III/II}$(DMSO) | 3.965 | 4.067 | 4.185 | 4.147 | 4.006 |

[a] Values in eV. For comparison, the reader must keep in mind that the OE for the Ag/AgCl reference electrode is close to 4.5 eV. [b] The processes listed are $Ru^{V/IV}$ and $Ru^{III/II}$. [c] The processes listed are $Ru^{IV/III}$ and $Ru^{III/II}$.

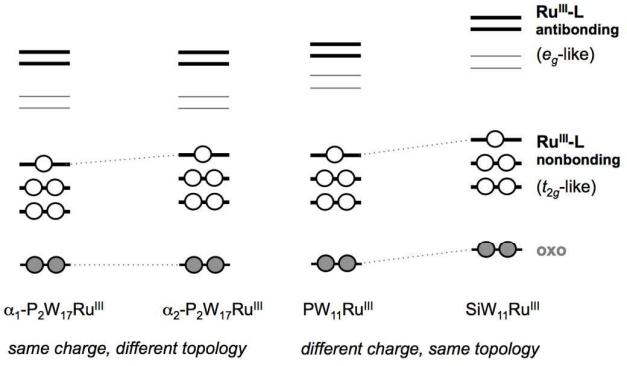


**Figure 8.** Schematic view of the energies (not scaled) and occupations of the oxo and Ru frontier molecular orbitals for (a) $\alpha_1$ and $\alpha_2$ Dawson and (b) P/Si-based Keggin Ru(III) compounds. Thick and think lines are Ru-like and W-like orbitals, respectively. Empty circles denote electrons occupying Ru-like orbitals.

In general, the sequence and energies of molecular orbitals explain the redox processes and their associated $\Delta E$s. For the $Ru^{III/II}$($H_2O$) couple, the orbital involved in the electron transfer (LUMO[59] of $Ru^{III}$ compound) is especially low in energy for $\alpha_1$-$P_2W_{17}$Ru and $PW_{11}$Ru: their BP86 energies are –4.37 eV and –4.36 eV, respectively. On the other hand, the LUMOs for

$GeW_{11}Ru^{III}(H_2O)$ (–4.17 eV) and $SiW_{11}Ru^{III}(H_2O)$ (–4.10 eV) are the highest ones. It is worth mentioning that the LUMOs of $Ru^{III}$(DMSO) compounds are invariably lower; for example, –4.53 eV and –4.54 eV for $\alpha_1$-$P_2W_{17}Ru$ and $PW_{11}Ru$, respectively. Such negative values explain the positive OEs listed in Table 2.

We can consider a relationship between the initial 'charge density' of the molecule and the redox energy (RE or OE). The charge density may be seen as the *q*/*m* ratio between the charge (*q*) and the size of a molecule —or the number of metal atoms, *m* in a simplified approach.[60] This ratio explains that the most negatively charged molecules of the series, the Dawson ones, are not the easiest to oxidize. Instead, $SiW_{11}Ru$ features the smallest $Ru^{III/II}$ OE, or less positive potential. Such a simple rule applies to POM compounds in general. Therefore, in order to reach the $Ru^{V}$(=O) state, higher negative molecular charges are wished since the associated OEs are less positive.

Another question is the origin of the OE differences for equally charged couples of compounds ($\alpha_1/\alpha_2$-$P_2W_{17}Ru$, or Ge/$SiW_{11}Ru$). Calculations certify again that the position of the Ru centre within Dawson anions (belt or cap) determines the oxidizing power, being the $\alpha_1$-isomer typically reduced more easily than the $\alpha_2$-isomer. The topological differences between these positions directly determine the energies of either molecular orbital.[48, 61] In the present case, the HOMO of $\alpha_1$-$P_2W_{17}Ru^{III}H_2O$ is 0.2 eV lower in energy than the homologous one of $\alpha_2$. In $\alpha_2$ systems, the homologous orbitals are slightly higher in energy due to their less delocalized nature and, thus, the oxidation process is more favourable if the electron is removed from the cap region (Supporting information, Figure S7). In a recent work[53] on Mo- and V-substituted Dawson systems, some of us showed that the molecular orbitals related to the belt-located substituting position are somewhat more delocalized over neighbouring metal centres, conferring extra stability to these electrons. Comparison of test calculations on fully electron-localized with electron-delocalized reduced systems showed that the energy stabilization related exclusively to electron delocalization in POM systems can reach 265 meV and 290 meV for Keggin and Dawson systems, respectively. This reasoning also explains why the reduced $P_2W_{18}$ system has electrons delocalized over *belt* tungstens.[61] In Keggin compounds, the relative redox behaviour of the equally charged Ge and Si derivatives arises from their different heteroatom sizes, as previously shown by DFT calculations.[62] Keggin anions with smaller internal heteroatoms (Si vs. Ge) feature less positive OEs (i.e., less positive oxidation potentials). This trend holds for the present Ru compounds. A graphical summary of the topological and charge effects can be found in Figure 8.

**Catalytic activity for water oxidation.** Development of an efficient and robust water oxidation catalyst (WOC) is one of the most important keys for realization of artificial photosynthesis, a presumable solution for worldwide energy concerns.[63-67] Water oxidation produces oxygen, protons and electrons (eq. 19), which are used for production of $H_2$ at a reduction catalyst (eq. 20). Oxygen evolution from water is a complex redox process, in which two water molecules and four electrons are involved, and is known to be the rate determining step.[68]

$$2\ H_2O \longrightarrow O_2 + 4\ H^+ + 4\ e^- \quad (19)$$
$$4\ H^+ + 4\ e^- \longrightarrow 2\ H_2 \quad (20)$$

POMs have attracted much attention as WOC catalysts.[64, 65, 69] Fukuzumi's group reported that mono-Ru-substituted Keggin-type silico- and germanotungstates with a terminal aqua ligand, $[SiW_{11}O_{39}Ru^{III}(H_2O)]^{5-}$ and $[GeW_{11}O_{39}Ru^{III}(H_2O)]^{5-}$, showed catalytic activity for water oxidation with cerium (IV) ammonium nitrate (CAN) as an oxidant.[8] They proposed that $Ru^{V}$(=O) species is an active intermediate. We reported that mono-Ru-substituted Keggin-type phosphotungstate with a terminal aqua ligand, $[PW_{11}O_{39}Ru^{III}(H_2O)]^{4-}$, showed catalytic activity for water oxidation.[9]

Figure 9 shows catalytic activities of **$\alpha_1$-$RuH_2O$** and **$\alpha_2$-$RuH_2O$** for water oxidation using CAN as an oxidant together with those of $[SiW_{11}O_{39}Ru^{III}(H_2O)]^{5-}$, $[PW_{11}O_{39}Ru^{III}(H_2O)]^{4-}$, and $[GeW_{11}O_{39}Ru^{III}(H_2O)]^{5-}$. All complexes are active for water oxidation, oxygen evolution is observed immediately after addition of CAN. Both **$\alpha_1$-$RuH_2O$** and **$\alpha_2$-$RuH_2O$** show slightly lower catalytic activity compared to those of $[SiW_{11}O_{39}Ru^{III}(H_2O)]^{5-}$, $[PW_{11}O_{39}Ru^{III}(H_2O)]^{4-}$, and $[GeW_{11}O_{39}Ru^{III}(H_2O)]^{5-}$, the initial reaction rates and total amount of generated oxygens of both **$\alpha_1$-$RuH_2O$** and **$\alpha_2$-$RuH_2O$** are lower than those of Keggin derivatives.

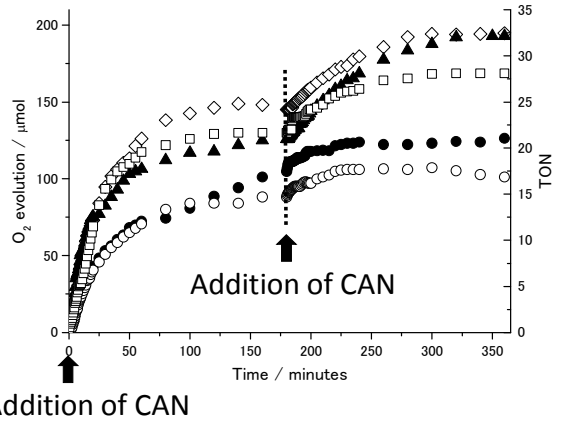


**Figure 9.** Oxygen evolution amount and turn over number plotted against time catalyzed by (closed circles) **$\alpha_1$-$RuH_2O$**, (open circles) **$\alpha_2$-$RuH_2O$**, (black triangles) $K_5[SiW_{11}O_{39}Ru(H_2O)]$, (open squares) $K_5[GeW_{11}O_{39}Ru(H_2O)]$, and (open diamonds) $Cs_4[PW_{11}O_{39}Ru(H_2O)]$. Mono-Ru-substituted heteropolytungstates (6 μmol) in 0.1 M $HNO_3$ (20 mL) in the presence of CAN (600 μmol). Black arrow indicates that addition of the second CAN (600 μmol).

**Thermal stability.** We measured thermal stabilities of five mono-Ru-substituted heteropolytungstates, **$\alpha_1$-$RuH_2O$**, **$\alpha_2$-$RuH_2O$**, $K_5[SiW_{11}O_{39}Ru(H_2O)]$, $K_5[GeW_{11}O_{39}Ru(H_2O)]$, and $Cs_4[PW_{11}O_{39}Ru(H_2O)]$ in air.

TG-DTA curves of **$\alpha_1$-$RuH_2O$** is similar to those of $K_5[SiW_{11}O_{39}Ru(H_2O)]$ and $K_5[GeW_{11}O_{39}Ru(H_2O)]$. There is a

weight loss up to ca. 200 °C which correspond to water evaporation, and there is an exothermal peak at ca. 546-580 °C (Supporting information, Figure S8). TG-DTA curves of **$\alpha_2$-$RuH_2O$** shows weight losses up to ca. 200 °C and between ca. 400 °C and 550 °C. In the case of $Cs_4[PW_{11}O_{39}Ru(H_2O)]$, there are two weight losses up to ca. 220 °C where the second weight loss is an exothermal reaction.

We heated these samples in air, and the heated samples were analyzed by cyclic voltammetry to estimate thermal stabilities (Supporting information, Figure S9). **$\alpha_1$-$RuH_2O$**, **$\alpha_2$-$RuH_2O$**, $K_5[SiW_{11}O_{39}Ru(H_2O)]$, $K_5[GeW_{11}O_{39}Ru(H_2O)]$, and $Cs_4[PW_{11}O_{39}Ru(H_2O)]$ are stable up to 400, 100, 500, 300, and 200 °C, respectively, and further heating results in decomposition. Among them **$\alpha_1$-$RuH_2O$** and $K_5[SiW_{11}O_{39}Ru(H_2O)]$ are highly stable under air.

## Conclusions

Isomerically pure $\alpha_1$- and $\alpha_2$-isomers of mono-Ru-substituted Dawson-type phosphotungstates, [$\alpha_1$- and $\alpha_2$-$P_2W_{17}O_{61}Ru^{III}(H_2O)]^{7-}$, were prepared by cleavage of the Ru-DMSO bond by hydrothermal treatment of [$\alpha_1$- and $\alpha_2$-$P_2W_{17}O_{61}Ru^{II}(DMSO)]^{8-}$ for the first time. The produced aqua complexes show proton-coupled electron transfer to produce $Ru^{IV}$(=O) and $Ru^{V}$(=O) species similar to mono-Ru-substituted Keggin derivatives. Electronic structure DFT calculations have shown that aqua compounds feature less positive oxidation energies than those of DMSO compounds, allowing them to reach the WOC active $Ru^{V}$(=O) state at lower potentials. This arises from the stronger Ru-$H_2O$ bonding conferring a stronger ligand field on the metallic orbitals that destabilize them more than the DMSO ligand. Both of the synthesized isomers [$\alpha_1$- and $\alpha_2$-$P_2W_{17}O_{61}Ru^{III}(H_2O)]^{7-}$ show catalytic activities as water oxidation catalysts. $K_7[\alpha_1\text{-}P_2W_{17}O_{61}Ru^{III}(H_2O)]$ and $K_5[SiW_{11}O_{39}Ru^{III}(H_2O)]$ are stable in air at temperatures more than 400 °C.

## Acknowledgements

This research was supported by the JST PRESTO program, Grants-in-Aid for Scientific Research (Scientific Research "C", grant no. 26420787) of the Ministry of Education, Culture, Sports, Science, Japan, the Spanish Ministry of Science and Innovation (MICINN) (project CTQ2011-29054-C02-01/BQU), the DGR of the Generalitat de Catalunya (grant no. 2014SGR199), and the XRQTC. We thank Ms. T. Amimoto at the Natural Science Center for Basic Research and Development (N-BARD), Hiroshima University for the measurement of ESI-MS measurement.

## Notes and references

1. L. Cronin, *Special Thematic Issue on Polyoxometalates, Chem. Soc. Rev.*, 2012, **41**, 7325-7648.
2. C. L. Hill, *Special Thematic Issue on Polyoxometalates, Chem. Rev.*, 1998, **98**, 1-390.
3. P. Putaj and F. Lefebvre, *Coord. Chem. Rev.*, 2011, **255**, 1642-1685.
4. N. V. Izarova, M. T. Pope and U. Kortz, *Angew. Chem. Int. Ed.*, 2012, **51**, 9492-9510.
5. A. Bagno, M. Bonchio, A. Sartorel and G. Scorrano, *Eur. J. Inorg. Chem.*, 2000, 17-20.
6. R. Neumann and C. Abu-Gnim, *J. Am. Chem. Soc.*, 1990, **112**, 6025-6031.
7. E. Steckhan and C. Kandzia, *Synlett*, 1992, 139-140.
8. M. Murakami, D. Hong, T. Suenobu, S. Yamaguchi, T. Ogura and S. Fukuzumi, *J. Am. Chem. Soc.*, 2011, **133**, 11605-11613.
9. S. Ogo, M. Miyamoto, Y. Ide, T. Sano and M. Sadakane, *Dalton Trans.*, 2012, **41**, 9901-9907.
10. M. Sadakane, N. Rinn, S. Moroi, H. Kitatomi, T. Ozeki, M. Kurasawa, M. Itakura, S. Hayakawa, K. Kato, M. Miyamoto, S. Ogo, Y. Ide and T. Sano, *Z. Anorg. Allgem. Chem.*, 2011, **637**, 1467-1474.
11. A. Sartorel, P. Miro, M. Carraro, S. Berardi, O. Bortolini, A. Bagno, C. Bo and M. Bonchio, *Chem. Eur. J.*, 2014, **20**, 10932-10943.
12. C. Rong and M. T. Pope, *J. Am. Chem. Soc.*, 1992, **114**, 2932-2938.
13. A. Yokoyama, K. Ohkubo, T. Ishizuka, T. Kojima and S. Fukuzumi, *Dalton Trans.*, 2012, **41**, 10006-10013.
14. J. C. Bart and F. C. Anson, *J. Electroanal. Chem.*, 1995, **390**, 11-19.
15. A. M. Khenkin, I. Efremenko, L. Weiner, J. M. L. Martin and R. Neumann, *Chem. Eur. J.*, 2010, **16**, 1356-1364.
16. D. Shi, C. He, B. Qi, C. Chen, J. Niu and C. Duan, *Chem. Sci.*, 2015, **6**, 1035-1042.
17. M. Sadakane, S. Moroi, Y. Iimuro, N. Izarova, U. Kortz, S. Hayakawa, K. Kato, S. Ogo, Y. Ide, W. Ueda and T. Sano, *Chem. Asia. J.*, 2012, **7**, 1331-1339.
18. S. Ogo, S. Moroi, T. Ueda, K. Komaguchi, S. Hayakawa, Y. Ide, T. Sano and M. Sadakane, *Dalton Trans.*, 2013, **42**, 7190-7195.
19. M. Sadakane, D. Tsukuma, M. H. Dickman, B. Bassil, U. Kortz, M. Higashijima and W. Ueda, *Dalton Trans.*, 2006, 4271-4276.
20. S. Ogo, N. Shimizu, T. Ozeki, Y. Kobayashi, Y. Ide, T. Sano and M. Sadakane, *Dalton Trans.*, 2013, **42**, 2540-2545.
21. K. Filipek, *Inorg. Chem. Acta*, 1995, **231**, 237-239.
22. B. Liu, J. Yan, Y.-F. Wang and X.-Y. Yi, *Dalton Trans.*, 2015, **44**, 16882-16887.
23. M. Sadakane, Y. Iimuro, D. Tsukuma, B. S. Bassil, M. H. Dickman, U. Kortz, Y. Zhang, S. Ye and W. Ueda, *Dalton Trans.*, 2008, 6692-6698.
24. K. Nishiki, H. Ota, S. Ogo, T. Sano and M. Sadakane, *Eur. J. Inorg. Chem.*, 2015, 2714-2723.
25. C. Vicent, S. A. Adonin, A. V. Anyushin, D. A. Mainichev and M. N. Sokolov, *Eur. J. Inorg. Chem.*, 2014, 5618-5624.
26. M. Sadakane, D. Tsukuma, M. H. Dickman, B. S. Bassil, U. Kortz, M. Capron and W. Ueda, *Dalton Trans.*, 2007, 2833-2838.
27. M. Sadakane and M. Higashijima, *Dalton Trans.*, 2003, 659-664.
28. C. Boglio, B. Hasenknopf, G. Lenoble, P. Rémy, P. Gouzerh, S. Thrimbert, E. Lacôte, M. Malacria and R. Thouvenot, *Chem. Eur. J.*, 2008, **14**, 1532-1540.
29. M. Sadakane, M. H. Dickman and M. T. Pope, *Inorg. Chem.*, 2001, **40**, 2715-2719.
30. W.-J. Xuan, C. Botuha, B. Hasenknopf and S. Thorimbert, *Chem. Eur. J.*, 2015, **21**, DOI: 10.1002/chem.201502839.
31. K. Nomiya, H. Torii, K. Nomura and Y. Sato, *J. Chem. Soc., Dalton Trans.*, 2001, 1506-1512.
32. S. Ogo, N. Shimizu, K. Nishiki, N. Yasuda, T. Mizuta, T. Sano and M. Sadakane, *Inorg. Chem.*, 2014, **53**, 3526-3539.
33. *ADF 2013.01, SCM, Theoretical Chemistry, Vrije Universiteit, Amsterdam, The Netherlands, http://www.scm.com*.

34. C. Fonseca Guerra, J. G. Snijders, G. Te Velde and E. J. Baerends, *Theor. Chem. Acc.*, 1998, **99**, 391-403.
35. G. Te Velde, F. M. Bickelhaupt, S. J. A. van Gisbergen, C. Fonseca Guerra, E. J. Baerends, J. G. Snijders and T. Ziegler, *Comput. Chem.*, 2001, **22**, 931-967.
36. A. D. Becke, *Rhys. Rev.*, 1988, **A38**, 3098-3100.
37. S. H. Vosko, L. Wilk and M. Nusair, *Can. J. Phys.*, 1980, **58**, 1200-1211.
38. J. P. Perdew, *Phys. Rev.*, 1986, **B33**, 8822-8824.
39. A. Klamt and G. Schüürmann, *J. Chem. Soc. Perkin Trans.*, 1993, **2**, 799-805.
40. J. Andzelm, C. Kölmel and A. Klamt, *J. Chem. Phys.*, 1995, **103**, 9312.
41. A. Klamt, *J. Phys. Chem.*, 1995, **99**, 2224-2235.
42. C. C. Implemented in the ADF package by Pye and T. Ziegler, *Theor. Chem. Acc.*, 1999, **101**, 396-408.
43. X. López, J. J. Carbó, C. Bo and J. M. Poblet, *Coord. Chem. Rev.*, 2012, **41**, 7537-7571.
44. C. T. Lee, W. T. Yang and R. G. Parr, *Phys. Rev. B*, 1988, **37**, 785-789.
45. P. J. Stephens, F. J. Devlin, C. F. Chabalowski and M. J. Frisch, *J. Phys. Chem.*, 1994, **98**, 11623-11627.
46. B. Keita, F. Girard and L. Nadjo, *J. Electroanal. Chem.*, 1999, **475**, 76-82.
47. A. J. Bard and L. R. Faulkner, *Electrochemical Methods*, Wiley, New York, 1980.
48. B. Keita, Y. Jean, B. Levy, L. Nadjo and R. Contant, *New J. Chem.*, 2002, **26**, 1314-1319.
49. J. P. Ciabrini, R. Contant and J. M. Fruchart, *Polyhedron*, 1983, **2**, 1229-1233.
50. S. P. Harmalker, M. A. Leparulo and M. T. Pope, *J. Am. Chem. Soc.*, 1983, **105**, 4286-4292.
51. M. Abbessi, R. Contant, R. Thouvenot and G. Hervé, *Inorg. Chem.*, 1991, **30**, 1695-1702.
52. B. Keita, I. M. Mbomekallé, L. Nadjo, P. de Oliveira, A. Ranjbari and R. Contant, *C. R. Chimie*, 2005, **8**, 1057-1066.
53. L. Parent, P. A. Aparicio, P. de Oliveira, A.-L. Teillout, J. M. Poblet, X. López and I. M. Mbomekallé, *Inorg. Chem.*, 2014, **53**, 5941-5949.
54. M. Sadakane and E. Steckhan, *J. Mol. Catal. A: Chem.*, 1996, **114**, 221-228.
55. M. Sadakane and E. Steckhan, *Chem. Rev.*, 1998, **98**, 219-237.
56. F. Doungmene, P. A. Aoaricio, J. Ntienoue, C. S. Ayingone Mezui, P. de Oliveira, X. López and I. M. Mbomekallé, *Electrochem. Acta*, 2014, **125**, 674-682.
57. *High spin configurations for Ru(III) and Ru(II) were also computed and obtained at notably higher energies.*
58. M. T. Pope and G. M. Varga, *Inorg. Chem.*, 1966, **5**, 1249-1254.
59. *HOMO: highest occupied molecular orbital; LUMO: lowest unoccupied molecular orbital.*
60. X. López, J. A. Fernández and J. M. Poblet, *Dalton Trans.*, 2006, 1162-1167.
61. X. López, C. Bo and J. M. Poblet, *J. Am. Chem. Soc.*, 2002, **124**, 12574-12582.
62. I. M. Mbomekallé, X. López, J. M. Poblet, F. Sécheresse, B. Keita and L. Nadjo, *Inorg. Chem.*, 2010, **49**, 7001-7006.
63. B. Limburg, E. Bouwman and S. Bonnet, *Coord. Chem. Rev.*, 2012, **256**, 1451-1467.
64. H. Lv, Y. V. Geletii, C. Zhao, J. W. Vickers, G. Zhu, Z. Luo, J. Song, T. Lian, D. G. Musaev and C. L. Hill, *Chem. Soc. Rev.*, 2012, **41**, 7572-7589.
65. A. Sartorel, M. Bonchio, S. Campanga and F. Scandol, *Chem. Soc. Rev.*, 2013, **42**, 2262-2280.
66. S. Fukuzumi and D. Hong, *Eur. J. Inorg. Chem.*, 2014, 645-659.
67. R. Cao, W. Lai and P. Du, *Energy Environ. Sci.*, 2012, **5**, 8134-8157.
68. H. Inoue, T. Shimada, Y. Kou, Y. Nabetani, D. Masui, S. Takagi and H. Tachibana, *ChemSusChem*, 2011, **4**, 173-179.
69. J. J. Stracke and R. G. Finke, *ACS Catal.*, 2014, **4**, 909-933.

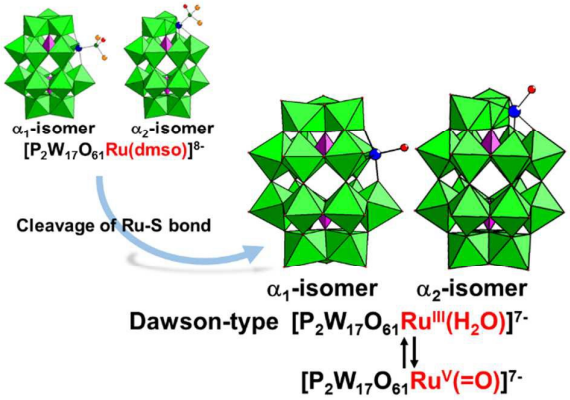


Synthesis of both $\alpha_1$- and $\alpha_2$-isomers of mono-Ru-substituted Dawson-type heteropolytungstates with a terminal aqua ligand and comparison of redox studies, thermal stabilities and catalytic activities for water oxidation with Keggin-derivatives.